Korean J. Chem. Eng., **21**(4), 821-828 (2004)

Adsorption and Regeneration Dynamic Characteristics of Methane and Hydrogen Binary System

Byoung-Uk Choi, Gi-Moon Nam, Dae-Ki Choi†, Byung-Kwon Lee, Sung-Hyun Kim* and Chang-Ha Lee**

Clean & Technology Center, Korea Institute of Science & Technology, P.O. BOX 131, Cheongryang, Seoul 130-650, Korea
*Department of Chemical and Biological Engineering, Korea University, Seoul 136-701, Korea
**Department of Chemical Engineering, Yonsei University, Seoul 120-749, Korea
(*Received 20 January 2003 • accepted 15 January 2004*)

Abstract−In order to optimize the performance of an adsorption column, the adsorption and regeneration dynamic characteristics were studied for 20% methane and 80% hydrogen binary system on nonisothermal and nonadiabatic conditions. The adsorption dynamic characteristics were studied at various flow rates, 7.2 LPM to15.8 LPM, and at various adsorption pressures, 6 to 12 atm. Also, regeneration dynamic characteristics were studied at various purge rates, 1.5 to 3.5 LPM, and constant pressure, 1.2 atm. Nonisothermal and nonadiabatic models, considering linear driving force model and Langmuir-Freundlich adsorption isotherm model, were considered to compare between prediction and experimental data.

Key words: Hydrogen, Methane, Adsorption, Regeneration, Dynamic

INTRODUCTION

Hydrogen is regarded as an ecologically clean and renewable energy source, and demands for hydrogen are on the rise from utilization in such fields as fuel cells, semiconductor processing and in the petrochemical industry. However, environmental regulations have been restricted so that CO_2-free hydrogen production process has been studied. For example, natural gas pyrolysis and plasma reaction process can produce CO_2-free hydrogen if they are operated in anoxic environment. But these products still include other impurities so that separation technology is necessary to produce high purity hydrogen. Adsorption separation technology is generally recognized as low in energy consumption with the added advantage of very precise (99.999%, H_2) component separation using pore size and surface characteristics of adsorbent [Ruthven, 1984; Yang, 1987]. Especially, the pressure swing adsorption (PSA) technology, which is attractive for its low energy requirements and low capital investment costs, is based on the physical phenomenon that the amount of a species that is adsorbed by an adsorbent increases as its partial pressure is raised. To design and model the PSA process, column dynamic characteristics are essential. In order to optimize the performance of the adsorption column, it is of foremost importance to understand the characteristics of adsorbent and adsorbate interactions in terms of thermodynamics and kinetics [Cho et al., 2004]. The dynamic characteristics of an adsorption column are affected by several factors and the most prominent ones may be the geometry of the adsorption column, operating scheme and conditions, characteristics of mass transfer, effects of adsorption heat, and the type of equilibrium isotherm. Adsorption modeling for a fixed bed system has been extensively studied for both isothermal [Garg et al., 1973, 1974a, b] and nonisothermal systems [Huang et al., 1988; Park, 2003; Sircar et al., 1983] and some papers for multicomponent adsorption modeling have been also reported [Choi et al., 2003; Na et al., 2001] Most of the models assume that the gas, regarded as ideal, is in the plug flow or plug flow with axial dispersion. The radial concentration and temperature gradients are neglected. In nonisothermal models thermal equilibrium is usually assumed to exist between the gas and solid phases. The adsorption equilibrium is described by using multicomponent isotherms; only rarely have linear isotherms been used. The gas-solid mass transport is usually modeled by the linear driving force (LDF) approximation [Yang et al., 2003]. The first and most widely used driving-force approximation was a linear one, derived by Glueckauf [Glueckauf et al., 1955]. Detailed discussions of the applications and limitation are given elsewhere [Hills et al., 1986; Yang, 1987]. The LDF model is a lumped-parameter model for particle adsorption. Malek and Farooq [Malek et al., 1996, 1997, 1998] used a constant LDF mass-transfer coefficient. In their study, it was particularly beneficial to model a multibed, multicomponent pressure swing adsorption process for hydrogen purification. The lumped-resistances mass transfer coefficients were generally treated as constants [Harwell et al., 1980; Wong et al., 1982]. Additionally, an energy balance is necessary for the bulk separation process because heat of adsorption/desorption causes temperature variation, 20-40 K, during adsorption and desorption. Especially, the temperature variation of more than 40 K occurred in a commercial unit [Cen et al., 1986; Kim et al., 2002]. So, if the temperature variation affects the adsorption isotherm significantly, severe error would occur if the energy balance was not taken into account because the nonisothermal case leads to adsorption at higher temperature and desorption at lower temperature, both of which reduce efficiency.

In this study, adsorption and regeneration column dynamic characteristics of methane and hydrogen binary system were studied. To model the column dynamics characteristics, nonisothermal and nonadiabatic conditions were considered and LDF model approxi-

†To whom correspondence should be addressed.
E-mail: dkchoi@kist.re.kr

mation adopted [Lee et al., 2003].

THEORY

In this study, an axially dispersed plug flow model was adopted and the linear driving force (LDF) approximation was used. Also, a complete nonisothermal and nonadiabatic dynamic model was adopted with the following assumptions:

(1) The ideal gas law applies.
(2) The flow pattern in the bed can be described by the axial dispersion plug flow model.
(3) The solid and gas phase reach thermal equilibrium instantaneously.
(4) Radial concentration and temperature gradients on the adsorption bed are negligible.
(5) Axial conduction in the wall can be neglected.
(6) The mass transfer rate is represented by a linear driving force expression.
(7) The multicomponent adsorption equilibrium is represented by the loading ratio correlation.

1. Material Balance

Using the flow pattern described by axial dispersion plug flow, the material balance for the bulk phase in the adsorption column is given by:

$$-D_L\frac{\partial^2 C_i}{\partial z^2}+\frac{\partial uC_i}{\partial z}+\frac{\partial C_i}{\partial t}+\frac{1-\varepsilon}{\varepsilon}\rho_p\frac{\partial \bar{q}}{\partial t}=0 \tag{1}$$

And overall mass balance can be written as:

$$-D_L\frac{\partial^2 C}{\partial z^2}+\frac{\partial uC}{\partial z}+\frac{\partial C}{\partial t}+\frac{1-\varepsilon}{\varepsilon}\rho_p\sum_{i=0}^{n}\frac{\partial \bar{q}_i}{\partial t}=0 \tag{2}$$

Where D_L is axial dispersion coefficient. It can be calculated by Wakao Eq. and followed:

$$\frac{D_L}{2uR_P}=\frac{20}{ReSc}+0.5 \tag{3}$$

In this model, the effects of all mechanisms which contribute to axial mixing are lumped together into a single effective axial dispersion coefficient, and it is possible to neglect axial dispersion and assume ideal plug model. However, when mass transfer resistance at the external film and/or within adsorbent particle is prominent at low feed rate, the weight of the axial dispersion term is increased, making this term important. If the ideal gas law applies to these equations, Eq. (1) and Eq. (2) can be transformed into:

$$-D_L\frac{\partial^2 y_i}{\partial z^2}+\frac{\partial y_i}{\partial t}+u\frac{\partial y_i}{\partial z}+\frac{RT}{P}\frac{1-\varepsilon}{\varepsilon}\rho_p\left(\frac{\partial \bar{q}_i}{\partial t}-y\sum_{j=1}^{n}\frac{\partial \bar{q}_i}{\partial t}\right)=0 \tag{4}$$

and the overall mass balance can be represented as follows:

$$-D_L\frac{\partial^2 P}{\partial z^2}+\frac{\partial P}{\partial t}+P\frac{\partial u}{\partial z}-PT\left(-D_L\frac{\partial^2(1/T)}{\partial z^2}+\frac{\partial(1/T)}{\partial t}+u\frac{\partial(1/T)}{\partial z}\right)+\frac{1-\varepsilon}{\varepsilon}\rho_P RT\sum_{j=1}^{n}\frac{\partial \bar{q}_i}{\partial t}=0 \tag{5}$$

2. Energy Balance

Assuming thermal equilibrium between fluid and particles, the energy balance for the gas and solid phase is given by:

$$-K_L\frac{\partial^2 T}{\partial z}+(\varepsilon_t\rho_g C_{pg}+\rho_B C_{ps})\frac{\partial T}{\partial t}+\rho_g C_{pg}\varepsilon u\frac{\partial T}{\partial z}-\rho_B\sum_{i}^{n}Q_i\frac{\partial \bar{q}_i}{\partial t}+\frac{2h_i}{R_{B_i}}(T-T_w)=0 \tag{6}$$

Where, $\varepsilon_t(\varepsilon+(1-\varepsilon)\varepsilon_p)$ is total void fraction and $\rho_B((1-\varepsilon)\rho_p)$ is bulk density. K_L is the effective axial thermal conductivity used for taking into account effective conduction in the axial direction. For the energy equation, effective axial thermal conductivity, K_L, can be estimated by using the empirical correlation given by Kunii and Smith [1960] and Yagi et al. [1964] as follows:

$$\frac{K_L}{k_g}=\frac{K_{L_0}}{k_g}+\delta Pr\,Re \tag{7}$$

$$\frac{K_{L_0}}{k_g}=\varepsilon+\frac{1-\varepsilon}{\varphi+\frac{2}{3}\frac{k_g}{k_s}} \tag{8}$$

$$\varphi=\varphi_2+(\varphi_1-\varphi_2)\left(\frac{\varepsilon-0.216}{0.216}\right)\ \text{for}\ 0.260\le\varepsilon\le0.476 \tag{9}$$

For all the simulations conducted in this study, the following parameter values were adopted:

$$(\delta,\varphi_1,\varphi_2)=(0.75, 0.2, 01) \tag{10}$$

In Eq. (6), the last term could be neglected causing heat transfer to wall to not be significant in comparison with the amount of heat from adsorption, if length-to-diameter is not large. However, since the diameter of the adsorption bed in the present study was rather small, heat loss through wall and heat accumulation in the wall could not be neglected. Therefore, an energy balance for the wall of the adsorption bed was constructed with the assumption of neglecting axial conduction in the wall:

$$\rho_w C_{pw}A_w\frac{\partial T_w}{\partial t}=2\pi R_{B_i}h_i(T-T_w)-2\pi R_{B_o}h_o(T-T_{atm}) \tag{11}$$

$$A_w=\pi(R_{B_o}^2-R_{B_i}^2) \tag{12}$$

3. Boundary Conditions

For a closed-closed system, the Danckwerts boundary conditions are applicable for the component balance. The boundary conditions and the initial conditions are in the following forms.

Boundary conditions at z=0 and z=L for fluid flow:

$$-D_L\left(\frac{\partial y_i}{\partial z}\right)\Big|_{z=0}=u(y_i|_{z=0^-}-y_i|_{z=0^+});\ \left(\frac{\partial y_i}{\partial z}\right)\Big|_{z=L}=0 \tag{13}$$

$$-K_L\left(\frac{\partial T}{\partial z}\right)\Big|_{z=0}=\rho_g C_{pg}u(T|_{z=0^-}-T|_{z=0^+});\ \left(\frac{\partial T}{\partial z}\right)\Big|_{z=L}=0 \tag{14}$$

where $y_i|_{z=0^-}$ means feed composition for component i

Velocity boundary condition at z=0 and z=L:

$$u|_{z=0}=u_0;\ \frac{\partial u}{\partial z}\Big|_{z=L}=0 \tag{15}$$

Initial condition for saturated bed:

$$C_i(z,0)=C_0;\ \bar{q}_i(z,0)=q_i^* \tag{16}$$

$$T(z,0)=T_{atm} \tag{17}$$

4. Adsorption Rate

Pore diffusion, surface diffusion, and solid diffusion are the representative diffusion mechanisms that are considered in this field. Also, intraparticle convection is considered for a large pore adsorbent, giving intermediate behavior of diffusion model and equilibrium model. However, it is very difficult to consider all the kinetic mechanisms for the purpose of representing sorption rate within adsorbent particles. The sorption rate into an adsorbent pellet is described by the following LDF model, which involves many possible mass transfer phenomena within a porous medium and external mass transfer into a single lumped mass transfer parameter, k [Ruthven et al., 1994]

$$\frac{\partial \bar{q}_i}{\partial t}=k_i(q_i^*-\bar{q}_i) \tag{18}$$

Where, q^* is the adsorbed-phase concentration in equilibrium with the local bulk phase concentration, and k is an LDF mass transfer coefficient, which can be estimated by the following equation:

$$\frac{1}{Kk}=\frac{R_P}{3k_f}+\frac{R_P^2}{15\varepsilon_P D_P}+\frac{r_c^2}{15KD_c} \tag{19}$$

Where, Eq. (19) is only applicable when the equilibrium is linear or at least not severely nonlinear and justified by an analysis of the moments of the dynamic response. Although the sorption model is rather simple, this rate model has been used extensively, regardless of adsorbate-adsorbent system in an equilibrium-controlled separation. This is because the adsorption process models using this sorption model predict experimental data with satisfactory accuracy [Panczyk et al., 2004].

The external film mass transfer coefficient, k_f, was used to calculate film resistance; the first term in Eq. (19), was determined by using the Wakao and Funazkri relation [Wakao et al., 1978]:

$$Sh=\frac{2R_P k_f}{D_m}=2.0+1.1Sc^{1/3}Re^{0.6} \text{ for } 0<Re<1000 \tag{20}$$

The second term in Eq. (19) was calculated by using the reciprocal addition law expression for molecular and Knudsen diffusion [Ruthven et al., 1984]:

$$\frac{1}{D_p}=\tau\left(\frac{1}{D_m}+\frac{1}{D_k}\right) \tag{21}$$

Where, τ is the tortuosity factor, which corresponds to straight, randomly oriented, cylindrical pores with equal probability of all possible orientations. The Knudsen and molecular diffusivities were calculated by using familiar expressions derived from the kinetic theory of gases [Ruthven et al., 1984].

5. Adsorption Isotherm

The Langmuir-Freundlich (L-F) isotherm was adopted for single component adsorption equilibrium, and the loading ratio correlation was considered to find proper multicomponent adsorption equilibrium parameters since the only noniterative method is the loading ratio correlation (LRC):

$$\text{L-F model } q=\frac{q_m BP^{1/n}}{1+BP^{1/n}} \tag{22}$$

$$\text{LRC model } q_i=\frac{q_{mi}B_iP_i^{1/n_i}}{1+\sum_{j=1}^{n}B_jP_j^{1/n_j}} \tag{23}$$

And the each LRC parameter was expressed to other parameters (k_1-k_6), respectively.

$$q_m=k_1+k_2T,\ B=k_3\exp(k_4/T),\ 1/n=k_5+k_6/T \tag{24}$$

6. Numerical Method

A finite difference method (FDM) was used to solve a mathematical model which consisted of coupled partial differential equations. A three-point backward finite difference approximation was used for temporal differential terms in order to improve temporal accuracy. The spatial dimension was discretized by using a second-order central difference and a second-order backward difference for the second-order and the first-order space derivatives, respectively [Hoffman et al., 1993; Wu et al., 1990]. The spatial grid spacing was 1 cm, where the time step was 0.02 sec. The conversion of model equations into algebraic equations using FDM leads to huge sparse matrix because dependent variables are coupled with each other. As a result, a great deal of computation time is required to solve the problem. Therefore, Yang and Doong [Yang et al., 1985] solved the equations separately in a sequential order to reduce the computation time in spite of a less accurate method. In this study, all the partial differential equations were converted into algebraic equations assuming the form of a trigonal matrix and the solutions were obtained by using the method of Yang and Doong [1985, 1986]. Then, computation results were used again through successive substitution until convergence was completed for a given time step. Accordingly, the coupled model equations could be solved in short computation time.

EXPERIMENTAL

1. Material

An adsorbent in this experimental was activated carbon (Calgon Co.). The physical properties tabulated in Table 1 are manufacturers report values. Prior to measurement, the adsorbent was maintained at 423.15 K in a drying vacuum oven more than 12 h to remove impurities. The adsorbates, and their purity, were methane 99.9% and hydrogen 99.9%.

2. Experiment Apparatus and Procedure

Table 1. Characteristics of activated carbon adsorbent

Type	Granular
Nominal pellet size	6-16 mesh
Average pellet size	0.115 mm
Pellet density	0.85 g/cm^3
Heat capacity	0.25 cal/gK
Particle porosity	0.61
Bulk density	0.532 g/cm^3
Bed porosity	0.433
Total void fraction	0.758

Table 2. Characteristics of adsorption bed

Length, L [cm]	120
Inside diameter, R_{B_i} [cm]	2.0447
Outside diameter, R_{B_o} [cm]	2.2073
Heat capacity of column, C_{pw} [cal/gK]	0.12
Density of column, ρ_w [g/cm^3]	7.83
Internal heat transfer coeffiecient, h_i [cal/cm^2·K·s]	0.00092
External heat transfer coefficient, h_o [cal/cm^2·K·s]	0.00034

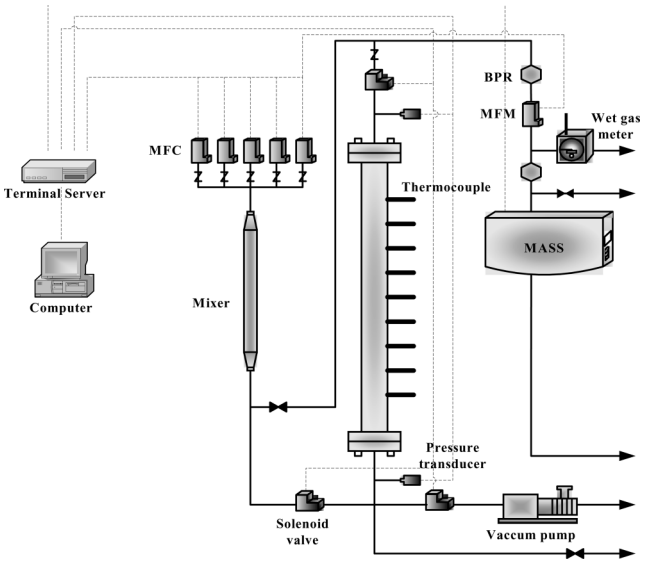

Fig. 1. Schematic diagram of breakthrough experiment apparatus.

A laboratory fixed bed adsorption and regeneration unit was used to study nonisothermal and nonadiabatic adsorption and regeneration for a hydrogen and methane (80/20) binary system on activated carbon adsorbent. A characteristic adsorption bed is represented in Table 2. A schematic diagram of the fixed-bed experimental setup is shown in Fig. 1. The column was fabricated from stainless steel and was 120 cm long with 4.1 cm inside diameter. The section in both ends of the column was filled with glass wool and metal screen to ensure uniform gas distribution and prevent the carryover of adsorbent particles. Nine K-type thermocouples were installed at 20, 30, 40, 50, 60, 70, 80, 90, and 100 cm from end of the column, and the temperature of the system was monitored and saved by DAS (data acquisition system). The gas flow to the column was controlled by a mass flow controller (Bronkhorst Co.) which was precalibrated against a soap bubble flow meter and checked by a wet gas meter. The system total pressure was controlled and maintained at a constant pressure with an electrical back-pressure regulator (Bronkhorst Co.), and was monitored with two pressure-transducers that were installed at both ends of the column. The sorbate concentration in the exit stream was detected continuously by mass spectrometer (Pfeiffer vacuum Ltd.). Also, the feed, which is hydrogen and methane (80/20), was premixed by mixer before the feed flow entered into the column. All of the units were operated by computer programmed by a visual basic language.

The adsorption dynamic characteristic experiments were conducted for hydrogen and methane (80/20) binary system on non-

Table 3. Adsorption dynamic characteristics experiment conditions

Run#	Flow rate [LPM]	Adsorption pressure [atm]
Run01	7.2	8
Run02	11.8	8
Run03	15.8	8
Run04	11.8	6
Run05	11.8	8
Run06	11.8	10
Run07	11.8	12

isothermal and nonadiabatic condition at various flow rates, 7.2-15.8 LPM (10-20 cm/s interstitial velocity), and at various adsorption pressures, 6-12 atm. Experimental conditions are represented in Table 3. Prior to experiment, activated carbon (Calgon, Co.) adsorbent was packed in a column after regeneration in a drying vacuum oven at 423.15 K more than 12 h to remove impurities, and weighing within ±10 mg accuracy. The packed column was evacuated by a high vacuum pump to remove a trace of impurity about more than 3 h. And then, it was purged with hydrogen. The required flow and the corresponding system pressure were adjusted with hydrogen and a sufficiently long time was allowed for the mass spectrometer until hydrogen mass fraction reached more than 99.99%. After that, feed flow entered into the column--this time was considered a starting point of experiment--and valves installed at each side of the column were opened simultaneously. Pressure and temperature in a column were recorded in DAS, and mass fraction of each component was also detected and recorded by a mass spectrometer.

As the same procedure, the regeneration dynamic characteristics experiments were conducted except pressurizing the column by using methane instead hydrogen at same condition of the adsorption dynamic characteristics experiment. Its experiments were conducted at various purge rates, 1.5-3.5 LPM, and at constant regeneration pressure, 1.2 atm. Its experimental conditions are represented in Table 4.

RESULTS AND DISCUSSION

1. Adsorption Equilibrium

The Langmuir-Freundlich (L-F) equation was employed for this system because the L-F equation predicted experimental data quite well. Additionally, the L-F isotherm has been widely used in modeling and designing of adsorption beds and periodic gas separation processes as they decrease calculation time [Malek et al., 1996]. On the other hand, for multi-component equilibria, the simpler extended versions of the single-component models provide adequate and numerically convenient means of predictions. The isotherm parame-

Table 4. Regeneration dynamic characteristics experiment conditions

Run#	Flow rate [LPM]	Regeneration pressure [atm]
Run01	1.5	1.2
Run02	2.5	1.2
Run03	3.5	1.2

Table 5. Loading ratio correlation model parameters for CH_4 and H_2 mixture onto activated carbon

	$k_1\times10^{-3}$	$k_2\times10^{-3}$	$k_3\times10^{-3}$	k_4	k_5	k_6	Q [cal/mol]
CH_4	23.86	−0.0562	2.81093	1220	1.628	−248.9	5625.18
H_2	7.34345	−0.013	0.932	506.306	0.586972	154.455	2880

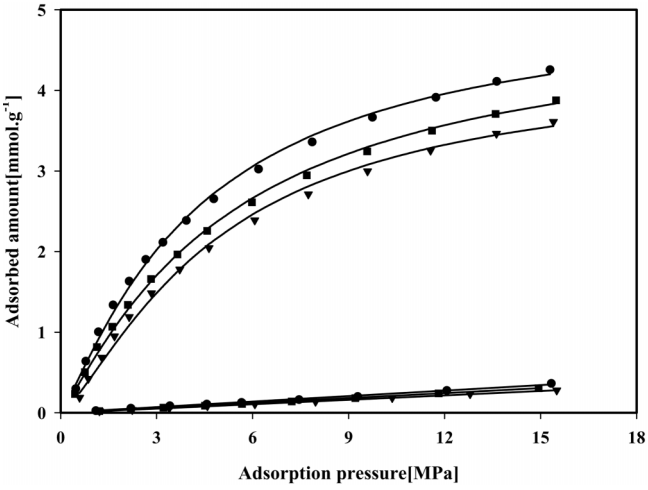

Fig. 2. Measured and fitted isotherms of CH_4 and H_2 onto activated carbon: ●, 293.15 K; ■, 303.15 K; ▼, 313.15 K; —, L-F model.

ters for the L-F equation are given in Table 5. When dealing with a multicomponent adsorption system, the reliable predictions of the adsorption equilibria are essential to properly analyze the dynamic behaviors of the adsorptive separation processes and to design and operate adsorption process system. But the experimental effort for measuring the mixture equilibrium isotherm requires too much time. So, several models exist in the literature for predicting adsorption of each component in a gas mixture from single gas isotherms. The LRC equations can be derived from the Langmuirian kinetic approach. Although its theoretical basis is not as rigorous as other models using the thermodynamic approach, it fits experimental data equally as well, as shown for activated carbon [Yang et al., 1985]. The L-F model parameters were used to calculate the LRC model parameters. The calculated LRC model parameters are in Table 5.

Isosteric heat of adsorption can be calculated by the Clausius-Clapeyron equation for adsorption. Usually, the isosteric heat of adsorption varies with surface coverage. Therefore, the relation between isosteric heat and coverage somewhat explains the surface structure. The isosteric heats of adsorption of methane and hydrogen were calculated by Clausius-Claypeyron equation (Table 5).

2. The Effect of Feed Velocity

Fig. 3 shows the effect of feed velocity and the predicted lines by the model considering LDF equation correspond relatively well with the experimental results. As shown in Fig. 3, the slower the feed velocity, the longer the breakthrough time. And the breakthrough time did not decrease linearly according to the linear increase in the feed velocity. It was confirmed that the difference in the breakthrough time between 7.2 LPM and 11.8 LPM became larger than between 11.8 LPM and 15.8 LPM. This implies that at least a certain amount of contact time was required due to the mass transfer resistance in the adsorbent. The predicted values fit quite well al-

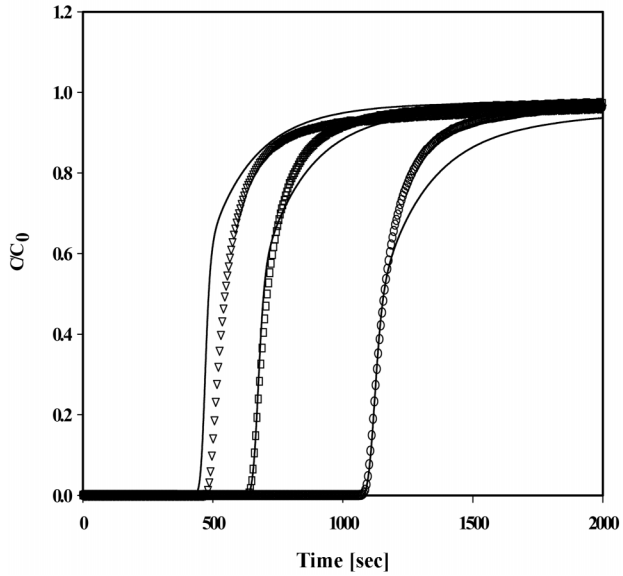

Fig. 3. CH_4 composition breakthrough curves for H_2/CH_4 system at 8 atm adsorption pressure: ○, 7.2 LPM; □, 11.8 LPM; ▽, 15.8 LPM; —, LDF model.

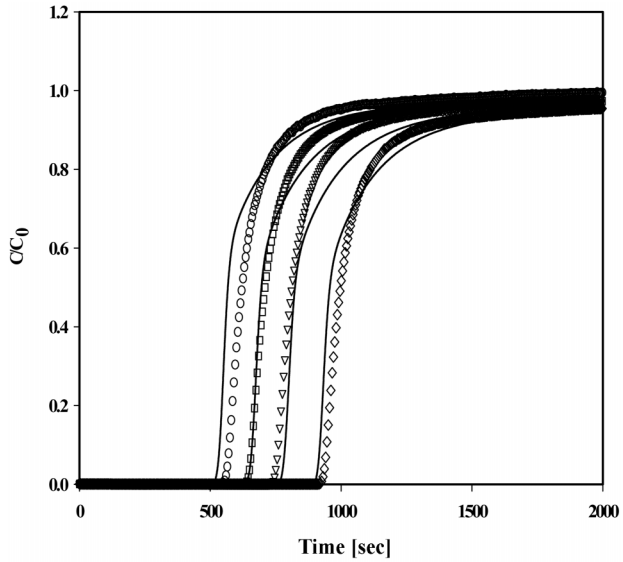

Fig. 4. CH_4 composition breakthrough curves for H_2/CH_4 system at 11.8 LPM flow rate: ○, 6 atm; □, 8 atm; ▽, 10 atm; ◇, 12 atm; —, LDF model.

though the predicted exit concentrations of methane were lower than actual values. This is due to the use of hydrogen and its competition for the surface sites. Thus, the adsorbed amount of methane as predicted by the model was longer than the actual time. Since more flow rate brings more adsorbates into the bed per unit time,

breakthrough is expected to be earlier.

3. The Effect of Adsorption Pressure

The experiments were performed at various pressures and at fixed flow rate. Fig. 4 shows the breakthrough curves according to the change of pressure at 11.8 LPM feed rate. The higher the pressure, the higher the adsorption capacity and the longer the breakthrough time became. Higher pressure will favor product purity of weak adsorbates but decrease the throughout or productivity. The predicted values were lower than actual values as the same reason for the case of the effect of flow velocity. For adsorption processes, a breakthrough time could be defined as the time when the effluent concentration of the adsorbate reaches half of its inlet concentration.

4. Temperature Variation During Adsorption

Typical temperature data measured at different height of the column, 20, 30, 40, 50, 60, 70, 80, 90, and 100 cm, during the experiments are shown in Fig. 5. As shown there, the temperature variation was large, about 20 K, for this system. It implies that energy balance equations must be included in modeling and the temperature curves demonstrate the importance of heats of adsorption in the gas adsorption process. The system temperature rose sharply due to the heat released by adsorption of methane on the activated carbon, and the system temperature then dropped until the energy demand was balanced with the energy supply, after which a temperature plateau was formed. Also, the temperature rises were slightly higher when the system pressure was high. From the equilibrium isotherm, it was clear that the bed loading capacity increased with the partial pressure of the adsorbate. Thus increasing the total pressure at a constant flow rate resulted in the higher temperature rises and later breakthrough of adsorbate. The temperature rise due to adsorption of adsorbate also could influence the breakthrough of solute. It is frequently reported that if the controlling resistance is macropore diffusion in the molecular regime, the mass transfer coefficient is inversely proportional to pressure, while within the Knudsen diffusion regime or conditions of micropore control, the mass transfer coefficient will be effectively independent of pressure [Raghavan et al., 1984; Ruthven et al., 1994]. The predicted temperatures tracked the experimental temperature profiles, but lower than the values. These differences can be explained in the following way. The radial heat conduction and heat conduction along the wall might be important in the apparatus used in the present study, but were neglected in the model. The heats of adsorption are functions of surface coverage, but were assumed constant in the whole range of operation. In addition, breakthrough time will be predicted by temperature breakthrough time the same as the concentration since temperature breakthrough point of the end of the column was very similar to concentration breakthrough point.

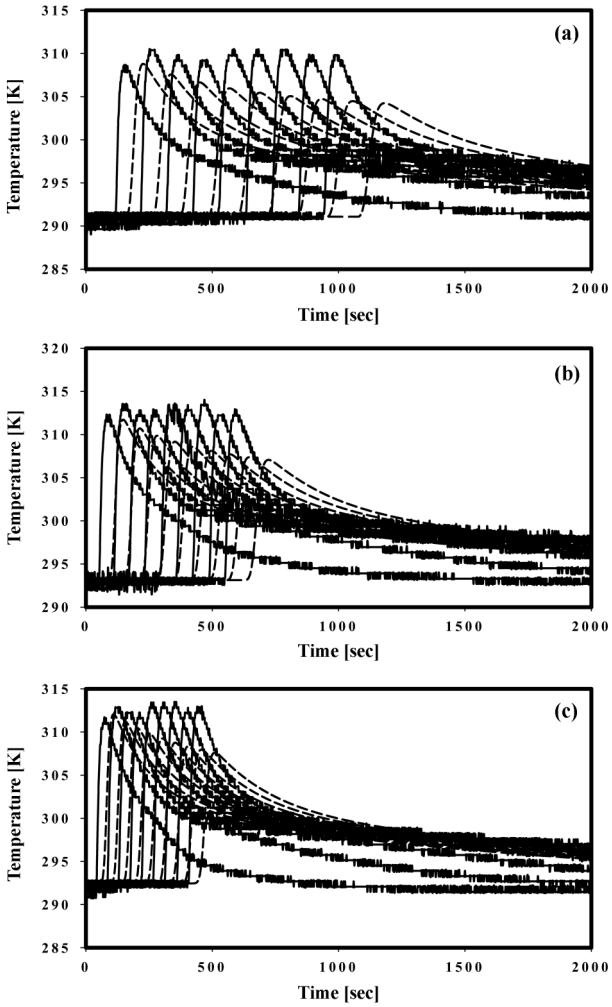

Fig. 5. Temperature variations for H_2/CH_4 system at 8 atm adsorption pressure: (a), 7.2 LPM; (b), 11.8 LPM; (c), 15.8 LPM; ---, LDF model.

5. Regeneration Dynamic Characteristics Results

Fig. 6 shows the regeneration breakthrough curves of methane of a bed saturated by methane at 1.2 atm. In the case of hydrogen, since the amount adsorbed at equilibrium was small, the desorption was done in a short of time as well. As the velocity of the hydrogen increased, the desorption was done even in a shorter period of time, but it was considered that the desorption was completed quickly because the effective diffusivity of hydrogen was large and

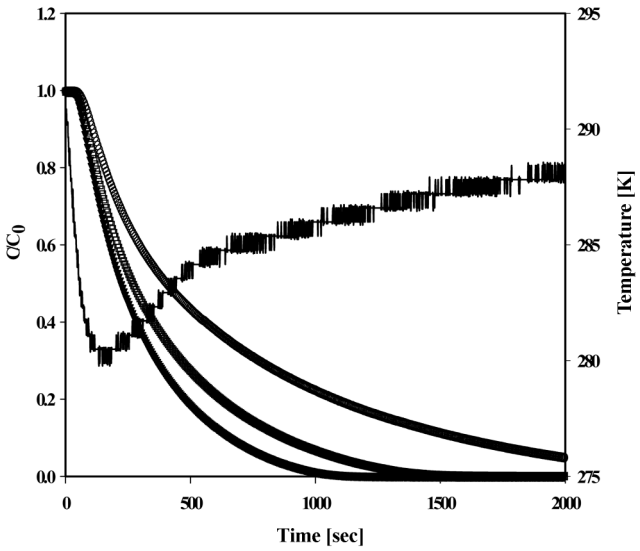

Fig. 6. Purge rate effect on H_2/CH_4 system at 1.2 atm blowdown pressure: ○, CH_4 conc. at 1.5 LPM; □, CH_4 conc. at 2.5 LPM; ▽, CH_4 conc. at 3.5 LPM; -, temperature variation at CH_4 conc. at 1.5 LPM.

the amount adsorbed with hydrogen at equilibrium on activated carbon was small. Temperature variations of the column entrance are shown in Fig. 6, which also shows the temperature variation was large, about 10 K, for this system.

CONCLUSIONS

In order to optimize the performance of the adsorption column, the adsorption and regeneration dynamic characteristics were studied for a 20% methane and 80% hydrogen binary system on non-isothermal and nonadiabatic conditions. The slower the feed velocity, the longer the breakthrough time, and the breakthrough time did not decrease linearly according to the linear increase in the feed velocity. The higher the pressure, the higher the adsorption capacity and the longer the breakthrough time became. The temperature variation was large, about 20 K, for this system. This implies that energy balance equations must be included in modeling and the temperature curves demonstrate the importance of heats of adsorption in the gas adsorption process. The predicted temperatures tracked the experimental temperature profiles, but with lower values than experimental values. These differences can be explained in the following way. Radial heat conduction and heat conduction along the wall might be important in the apparatus used in the present study, but were neglected in the model. The regeneration breakthrough curves of methane of a bed saturated by methane at 1.2 atm. As the velocity of the hydrogen increased, the desorption was done even in a shorter period of time.

ACKNOWLEDGMENT

This work was supported by LNG Technology Research Center, Korea Gas Corporation and the Ministry of Commerce, Industry and Energy.

NOMENCLATURE

A_w : cross sectional area [cm^2]
C : concentration of adsorbate [mol/g]
C_0 : initial concentration of adsorbate [mol/g]
C_{pg} : gas heat capacity [cal/gK]
C_{ps} : particle heat capacity [cal/gK]
C_{pw} : bed wall heat capacity [cal/gK]
D_k : Knudsen diffusivity [cm^2/s]
D_L : mass axial dispersion coefficient [cm^2/s]
D_m : molecular diffusivity [cm^2/s]
D_P : intraparticle diffusivity [cm^2/s]
h : heat transfer coefficient [$cal/cm^2 \cdot s \cdot K$]
k : linear driving force mass transfer coefficient [s^{-1}]
$k_{1\text{-}6}$: loading ratio correlation isotherm model parameter
k_f : external film mass transfer coefficient [cm/s]
k_g : thermal conductivity of fluid [$cal/cm^2 \cdot s \cdot K$]
k_s : thermal conductivity of particle [$cal/cm^2 \cdot s \cdot K$]
K : equilibrium constant [q^*/C_0] Henry's law adsorption equilibrium constant
K_L : effective axial thermal conductivity [$cal/cm^2 \cdot s \cdot K$]
K_{L_0} : initial effective axial thermal conductivity [$cal/cm^2 \cdot s \cdot K$]
P : pressure [atm]
Pr : Prandtl number [$C_{pg}\mu/k_g$]
q : equilibrium moles adsorbed [mol/g]
q_m : maximum equilibrium moles adsorbed [mol/g]
q_{st} : isosteric heat of adsorption [kJ/mol]
$\bar{q}$: volume-averaged adsorbed phase concentration [mol/g]
q^* : equilibrium adsorbed phase concentration [mol/g]
Q : average isosteric heat of adsorption [cal/mol] or volumetric flow rate [cm^3/s]
r_P : single particle radius [cm]
R : gas constant [cal/molK]
R_B : bed radius [cm]
R_P : particle radius [cm]
Re : Reynolds number [$\rho_g u(2R_P)/\mu$]
Sc : Schmidt number [$\mu\rho_g/D_m$]
t : time [s]
T : temperature [K]
T_{atm} : ambient temperature [K]
T_w : wall temperature [K]
u : interstitial velocity [cm/s]
u_0 : initial interstitial velocity [cm/s]
V : volume [cm^3]
y : mole fraction in gas phase
z : axial position in a adsorption bed [cm]

Greek Letters

ε : interparticle void fraction
ε_t : total void fraction
ρ_B : bulk density [cm^3/g]
ρ_g : gas density [cm^3/g]
ρ_p : particle density [cm^3/g]
ρ_w : bed density [cm^3/g]
δ : parameters used in Eq. (7)
φ : parameters used in Eq. (8)
τ : tortuosity factor

REFERENCES

Cen, P. and Yang, R. T., "Bulk Gas Separation by Pressure Swing Adsorption," *Ind. Eng. Chem. Fundam*., **25**, 758 (1986).

Choi, W. K., Kwon, T. I. and Yeo, Y. K., "Optimal Operation of the Pressure Swing Adsorption (PSA) Process for CO_2 Recovery," *Korean J. Chem. Eng.*, **20**(4), 617 (2003).

Cho, Y. S., Cho, S. I. and Heo, J. S., "Thermodynamic Analysis of Liquid Source Chemical Vapor Deposition Process for the Preparation of a Ba-Sr-Ti Oxide Film," *Korean J. Chem. Eng.*, **21**(1), 286 (2004).

Garg, D. R. and Ruthven, D. M., "Theoretical Prediction of Breakthrough Curves for Molecular Sieve Adsorption Column-II General Isotherm Solution for Micropore Diffusion Control," *Chem. Eng. Sci.*, **28**, 799 (1973).

Garg, D. R. and Ruthven, D. M., "The Performance of Molecular Sieve Adsorption Column: Systems with Macropore Diffusion Control," *Chem. Eng. Sci*., **29**, 1961 (1974a).

Garg, D. R. and Ruthven, D. M., "The Performance of Molecular Sieve Adsorption Column: Systems with Micropore Diffusion Control," *Chem. Eng. Sci*., **29**, 571 (1974b).

Glueckauf, E., "Formulas for Diffusion into Sphere and Their Application to Chromatography," *Trans. Faraday Soc*., **51**, 1540 (1955).

Harwell, J. H., Liapis, A. I., Lichtfield, R. and Hanson, D. T., "A Non-Equilibrium Model for Fixed-Bed Multicomponent Adiabatic Adsorption," *Chem. Eng. Sci*., **35**, 2287 (1980).

Hills, J. H., "An Investigation of the Linear Driving Force Approximation to Diffusion in Spherical Particles," *Chem. Eng. Sci*., **41**, 2779 (1986).

Hoffman, K. A. and Chiang, S. T., "Computational Fluid Dynamics for Engineers," A Publication of Engineering Education System, Wichita (1993).

Huang, C. C. and Fair, J. R., "Study of the Adsorption and Desorption of Multiple Adsorbates in a Fixed Bed," *AIChE J*., **34**, 1861 (1988).

Kunii, D. and Smith, J. M., "Heat Transfer Characteristics of Porous Rocks," *AIChE J*., **6**, 1, 71 (1960).

Kim, S. J., Shim, W. G. and Kim, T. Y., "Adsorption Equilibrium Characteristics of 2,4-Dichlorophenoxyacetic Acid and 2,4-Dinitrophenol on Granular Activated Carbons," *Korean J. Chem. Eng.*, **19**(6), 967 (2002).

Lee, W. K. and Ko, J. S., "Kinetic Model for the Simulation of Hen Egg White Lysozyme Adsorption at Solid/Water Interface," *Korean J. Chem. Eng.*, **20**(3), 549 (2003).

Malek, A. and Farooq, S. J., "Determination of Equilibrium Isotherms using Dynamic Column Breakthrough and Constant Flow Equilibrium Desorption," *Chem. Eng. Data*., **41**, 25 (1996).

Malek, A. and Farooq, S., "Kinetic of Hydrocarbon Adsorption on Activated Carbon and Silica Gel," *AIChE J*., **43**(3), 761 (1997).

Malek, A. and Farooq, S., "Hydrogen Purification from Refinery Fuel Gas by Pressure Swing Adosrption," *AIChE J*., **44**(9), 1985 (1998).

Na, B. K., Koo, K. K. and Eum, H. M., "CO_2 Recovery from Flue Gas by PSA Process using Activated Carbon," *Korean J. Chem. Eng.*, **18**(2), 220 (2001).

Panczyk, T. and Rudzinski, W., "Kinetics of Gas Adsorption on Strongly Heterogeneous Solid Surfaces: A Statistical Rate Theory Approach," *Korean J. Chem. Eng.*, **21**(1), 206 (2004).

Park, J. K., Kim, S. J. and Lee, J. W., "Adsorption Selectivity of Phenylalanine Imprinted Polymer Prepared by the Wet Phase Inversion Method," *Korean J. Chem. Eng.*, **20**(6), 1066 (2003).

Raghavan, N. S. and Ruthven, D. M., "Dynamic Behavior of an Adiabatic Adsorption Column-II. Numerical Simulation and Analysis of Experimental Data," *Chem. Eng. Sci*., **39**, 1201 (1984).

Ruthven, D. M., "Principles of Adsorption and Adsorption Processes," John Wiley & Sons, New York (1984).

Ruthven, D. M., Farooq, S. and Knaebel, K. S., "Pressure Swing Adsorption," VCH publishers, New York (1994).

Sircar, S. and Kurma, R., "Adiabatic Adsorption of Bulk Binary Gas Mixtures: Analysis by Constant Pattern Model," *Ind. Eng. Chem. Process Des. Dev.*, **22**, 271 (1983).

Sircar, S. and Kurma, R., "Column Dynamics for Adsorption of Bulk Binary Gas Mixtures on Activated Carbon," *Sep. Sci. Tech*., **21**, 919 (1986).

Wakao, N. and Funazkri, T., "Effect of Fluid Dispersion Coefficients on Particle-to-Fluid Mass Transfer Coefficients in Packed Beds," *Chem. Eng. Sci*., **33**, 1375 (1978).

Wong, Y. W. and Niedzwiecki, J. L., "A Simplified Model for Multicomponent Fixed Bed Adsorption," *AIChE Symp. Ser.*, **78**, 219 (1982).

Wu, J. C., Fan, L. T. and Erickson, L. E., "Three-point Backward Finite-difference Method for Solving a System of Mixed Hyperbolic-parabolic Partial Differential Equations," *Computers Chem. Engng*., **14**, 679 (1990).

Yagi, S. and Kunii, D., "Studies on Heat Transfer Near Wall Surface in Packed Beds," *AIChE J*., **6**, 1, 97 (1964).

Yang, R. T., "Gas Separation by Adsorption Processes," Butter Worths (1987).

Yang, R. T. and Doong, S. J., "Gas Separation by Pressure Swing Adsorption: A Pore-Diffusion Model for Bulk Separation," *AIChE J*., **31**, 1829 (1985).

Yang, R. T. and Doong, S. J., "Bulk Separation of Multicomponent Gas Mixtures by Pressure Swing Adsorption: Pore/Surface Diffusion and Equilibrium Models," *AIChE J*., **32**, 397 (1986).

Yang, W. C., Shim, W. G. and Lee, J. W., "Adsorption and Desorption Dynamics of Amino Acids in a Nonionic Polymeric Sorbent XAD-16 Column," *Korean J. Chem. Eng.*, **20**(5), 922 (2003).